HHS Public Access

Author manuscript

Phys Med Biol. Author manuscript; available in PMC 2022 January 26.

Published in final edited form as:

Phys Med Biol. ; 66(3): 035013. doi:10.1088/1361-6560/abcb1e.

Characterizing Blood Clots Using Acoustic Radiation Force Optical Coherence Elastography and Ultrasound Shear Wave Elastography

Hsiao-Chuan Liu[1], **Mehdi Abbasi**[1], **Yong Hong Ding**[1], **Tuhin Roy**[2], **Margherita Capriotti**[1], **Yang Liu**[1], **Seán Fitzgerald**[1,3], **Karen M. Doyle**[3], **Murthy Guddati**[2], **Matthew W. Urban**[1,4], **Waleed Brinjikji**[1]

[1]Department of Radiology, Mayo Clinic, 200 First St SW, Rochester, MN 55905, USA
[2]Department of Civil Engineering, North Carolina State University, Raleigh, NC 27695, USA
[3]Department of Physiology, National University of Ireland Galway, Galway, Ireland [4]Department of Physiology and Biomedical Engineering, Mayo Clinic, 200 First St SW, Rochester, MN 55905, USA

Abstract

Thromboembolism in a cerebral blood vessel is associated with high morbidity and mortality. Mechanical thrombectomy (MT) is one of the emergency procedures performed to remove emboli. However, the interventional approaches such as aspiration catheters or stent retriever are empirically selected. An inappropriate selection of surgical devices can influence the success rate during embolectomy, which can lead to an increase in brain damage. There has been growing interest in the study of clot composition and using *a priori* knowledge of clot composition to provide guidance for an appropriate treatment strategy for interventional physicians. Developing imaging tools which can allow interventionalists to understand clot composition could affect management and device strategy. In this study, we investigated how clots of different compositions can be characterized by using acoustic radiation force optical coherence elastography (ARF-OCE) and compared with ultrasound shear wave elastography (SWE). Five different clots compositions using human blood were fabricated into cylindrical forms from fibrin-rich (21% red blood cells, RBCs) to RBC-rich (95% RBCs). Using the ARF-OCE and SWE, we characterized the wave velocities measured in the time-domain. In addition, the semi-analytical finite element model was used to explore the relationship between the phase velocities with various frequency ranges and diameters of the clots. The study demonstrated that the wave group velocities generally decrease as RBC content increases in ARF-OCE and SWE. The correlation of the group velocities from the OCE and SWE methods represented a good agreement as RBC composition is larger than 39%. Using the phase velocity dispersion analysis applied to ARF-OCE data, we estimated the shear wave velocities decoupling the effects of the geometry and material properties of the clots. The study demonstrated that the composition of the clots can be characterized by elastographic methods using ARF-OCE and SWE, and OCE demonstrated better ability to discriminate between

Disclosures

The authors declare that there are no conflicts of interest related to this article.

clots of different RBC compositions, compared to the ultrasound-based approach, especially in clots with low RBC compositions.

1. Introduction

Ischemic stroke is a major cause of mortality and morbidity worldwide with close to 700,000 cases per year in the United States (Das *et al.*, 2012). It is an aetiologically heterogeneous disease, and proper treatment mandates timely intervention (Montaner *et al.*, 2008; Donnan *et al.*, 2008; Grau *et al.*, 2001). Ischemic stroke secondary to large vessel occlusion is the most devastating form of acute ischemic stroke and accounts for 10–20% of all ischemic strokes. Since 2015 there have been several randomized controlled trials which have shown that endovascular thrombectomy, a procedure in which catheters are introduced to the cerebral arteries and the clot is retrieved, is an effective treatment for large vessel occlusion stroke (Goyal *et al.*, 2016; Powers *et al.*, 2015). However, despite advancements in technology, the rate of complete recanalization remains close to 60% (Goyal *et al.*, 2016; Powers *et al.*, 2015).

Over the last couple of years, our knowledge on the thromboembolus histology, mechanical properties and effects of these properties on the success of mechanical thrombectomy (MT) has grown (Hashimoto *et al.*, 2016; Undas *et al.*, 2010). There is growing evidence supporting a relationship between selecting an appropriate surgical device during MT (aspiration catheter versus stent-retriever device) and histological composition of clots. There is a strong association between the histological composition of clots and their mechanical properties. (Raychev and Saver, 2012) (Brinjikji *et al.*, 2020). *In vitro* studies have shown that fibrinous clots are generally stiffer than red blood cell (RBC)-rich clots, which can make them harder to remove with conventional techniques. However, selecting an appropriate surgical device during MT is empirical by neurointerventionalists. Although immunostaining has been widely performed to identity compositions of clots as the gold-standard method, this process is time-consuming and it is subject to inter- and intra-observer variability as images are interpreted (Jorgensen *et al.*, 2017). Therefore, understanding the mechanical properties of clots with multiple RBC compositions can play a pivotal role in choosing an appropriate surgical device to increase success rate of MT and can also be useful for determining the etiology of these pathologies.

During the last decade, optical coherence tomography (OCT) has been utilized to investigate mechanical properties of biological tissues and fluids due to a number of advantages: noninvasive and noncontact, high spatial resolution, fast, and sensitive to the topology of a surface (Wang and Larin, 2015; Razani *et al.*, 2012; Liu *et al.*, 2020b, a). An extended technology of OCT to evaluate viscoelasticity and mechanical response of localized bio-samples by measuring their internal or surface motion produced from various excitations is called optical coherence elastography (OCE). Previous studies have demonstrated that OCE has capability to characterize mechanical properties of skin (Li *et al.*, 2012b), chicken breast (Li *et al.*, 2012a), rat tumor tissue (Liang *et al.*, 2010), prostate cancer (Li *et al.*, 2015) and lens/cornea especially (Kirby *et al.*, 2017; Ambrozinski *et al.*, 2016; Wang and Larin, 2015; Manapuram *et al.*, 2011; Han *et al.*, 2015; Han *et al.*, 2017). Recently, quantifying

mechanical properties of blood coagulation has been studied by using OCE because abnormal mechanical properties of clots correspond with the risk of thrombosis and bleeding; therefore, quantifying mechanical properties of coagulation is able to provide information about hemorrhage prognosis, to guide hemostatic therapies and to predict the risk of bleeding during surgical procedures (Xu *et al.*, 2019; Xu *et al.*, 2016).

Ultrasound shear wave elastography (SWE) uses focused ultrasound beams to produce acoustic radiation force (ARF), which causes the tissue to displace and shear waves to propagate lateral to the push (Sarvazyan *et al.*, 1998; Doherty *et al.*, 2013; Urban, 2018). The velocity of the propagating waves is related to the mechanical properties of the tissue, with tissues with higher stiffness or modulus yielding faster velocities. SWE has been used in many different tissues (Sarvazyan *et al.*, 2011), but sparingly for evaluation of coagulating blood and blood clots. (Mfoumou *et al.*, 2014; Liu *et al.*, 2017). Previous research has reported that ultrasound is a useful tool in assessing deep vein thrombosis (DVT) by using acoustic radiation force (ARF) (Viola *et al.*, 2004; Wang *et al.*, 2015) and ultrasound strain elastography (Hoang *et al.*, 2017; Rubin *et al.*, 2003; Rubin *et al.*, 2006; Xie *et al.*, 2005). Several studies have been conducted using SWE to investigate how the viscoelastic properties of blood changes during coagulation (Bernal *et al.*, 2012, 2013; Schmitt *et al.*, 2011; Bhatt *et al.*, 2018). Clot mechanical properties were recently investigated using SWE techniques in the context of thrombolysis (Mercado-Shekhar *et al.*, 2018). Clot stiffness has also been investigated in an animal model of venous thrombosis (Mfoumou *et al.*, 2014; Liu *et al.*, 2017).

Evaluating human thrombus with various RBC compositions using elastographic methods has not been widely reported yet. As devices are developed specifically for dealing with fibrin-rich clots, it is becoming increasingly important to develop techniques to characterize clot histological and physical properties *in vivo* (Benson *et al.*, 2020; Fennell *et al.*, 2018). Understanding the mechanical properties of clots with various RBC compositions can play a pivotal role in choosing an appropriate surgical device to increase success rate of MT and can also be useful for determining the etiology of these pathologies. RBC-rich clots are more prone to fragmentation potentially leading to distal embolization, whilst fibrin/platelet-rich clots are more difficult to retrieve. In this paper, we used both OCE and SWE to differentiate clots with multiple red blood cell (RBC) compositions. The clots fabricated using healthy human whole blood in the study are consistent with the clots in patients with intracranial large vessel occlusion. The wave velocities are compared among the different methods as well trying to estimate the shear modulus of the clots. OCE and SWE are potential modalities to be used for *in situ* clots when combined with endovascular catheters for clinical translation.

2. Materials and Methods

2.1 Clot Analogues Preparation Protocol

Following Institutional Review Board (IRB) approval from Mayo Clinic, human whole blood was obtained from the Blood Transfusion Service. Blood was centrifuged at 1200 RPM for 20 minutes at 20°C which resulted in separation of Blood into plasma, buffy-coat, and erythrocyte-rich layers. The plasma and erythrocytes (RBCs) were collected

independently and then recombined in controlled ratios inside the 50 mL Falcone tube to make five different types of clot analogues (3 analogues for each type). A 2.06% calcium chloride (Sigma Aldrich, Product No: C1016) and 2% thrombin (Sigma Aldrich, Product No: 10602400001) were also added to facilitate the formation of clots. Solution inside each tube was mixed by 5 times inversion and then was quickly drawn into 3 ml syringes. For this study, 5 types of clot analogues were included with increasing concentrations of RBCs. Group 1: most fibrin-rich; Group 2: fibrin-rich; Group 3: mixed; Group 4: RBC-rich and Group 5: most RBC-rich. The clots were approximately cylindrically shaped though the diameter changed based on the RBC content. All clots were made in 3 mL syringes. The length of the clots was approximately 30 mm for all clots. The diameter of the clots changed as a function of RBC content. Analogues were prepared 4 hours before the experiment and they were stored at room temperature (26°C). Selection of the concentration of the RBCs used in this study is based on clinical data. In our clinical experiences, the RBC composition ranges from 5–80%. Therefore, selecting 20–25% as an interval was appropriate to cover this range. The terminal cases were selected as 5% and 95% RBC composition because 0% and 100% RBC compositions in clots did not exist in our clinical cases.

2.2 Histologic Analysis

Following our experiments, each clot analogue was fixed in 10% phosphate-buffered formalin (Thermo-Scientific, Product No: 5701) for 2 days and then clot analogues were processed and embedded in paraffin. Formalin fixed paraffin embedded analogues were sectioned into 3 μm slices and then a representative slide of each analogue was stained with Martius Scarlett Blue trichrome (MSB). Histological quantification was performed using Orbit Image Analysis software (https://www.orbit.bio/, licensed under GPLv3) (Fitzgerald *et al.*, 2019). The percentage of components including RBC, fibrin and platelets was determined.

2.3 Acoustic Radiation Force Optical Coherent Elastography (ARF-OCE)

The acoustic radiation force optical coherence tomography (ARF-OCT) system used to perform the OCE measurements is composed of a spectral domain OCT (SD-OCT) scanner with a 1300 nm central wavelength (TEL320C1, Thorlabs Inc., Newton, NJ, USA), a 7.5 MHz focused transducer (ISO703HR, Valpey-Fisher, Hopkinton, MA, USA), three function generators (33250A, Agilent, Santa Clara, CA, USA) and a radiofrequency (RF) amplifier (240L, Electronics and Innovation, LTD, Rochester, NY, USA), illustrated in Fig. 1. The OCT system is capable of producing 13 μm lateral resolution within a 10 mm × 10 mm field-of-view (FOV) to detect the motion of particles inside the clots. The penetration depth will be governed by the level of optical scattering and absorption for a given sample. For the deepest imaging depth in clots with 95% RBC composition as an example, the penetration depth is approximately 0.5 mm based on our experiments. To capture the propagation of waves from the various compositions of clots, the M-B scan mode with 10 kHz scan rate was used to track dynamic processes in the spatiotemporal domain.

A customized acquisition of 100 lateral positions and 500 axial scans was set to obtain in-phase/quadrature (IQ) data using the OCT. The 2 ms ARF excitation was repeated every 50 ms to exert force on the clots for generating wave propagation and the focal point was placed

on the top of the clots to provide good momentum transfer. Once removed from the syringe, the clot was positioned over the transducer on a Petri dish with a Mylar layer replacing the plastic to reduce ultrasonic attenuation and reverberation. The driving voltage was set as 100 mV from a function generator and was applied to the RF amplifier before applying to the transducer to generate shear waves. Please note that, for clots with 5% RBC composition, the driving voltage was set as 400 mV to generate Rayleigh waves due to their much higher optical transparency compared to other clots. The autocorrelation was used to search maximum of the motion signal and time of that peak at each spatial location in order to create a two-dimensional (2D) lateral time-peak wave map for evaluating shear wave motions. For the fibrin-rich clots, the Raleigh wave motions were considered by utilizing cross-correlation algorithm to obtain lateral time-peak wave map, and a median filter was employed to remove noise from a 2D wave motion map before performing cross-correlation (Liu *et al.*, 2020a). In this study, each RBC composition contains three individual samples, and ten acquisitions were performed for each sample.

2.4 Shear Wave Elastography (SWE)

After OCE measurement, the ultrasound SWE measurements were performed on the same clots. The clots were placed in a saline bath on a rubber pad. Each clot was pinned to the rubber to prevent motion, but care was taken to avoid stretching the clots. To make SWE measurements, we utilized a programmable ultrasound scanner (V1, Verasonics, Inc., Kirkland, WA) and a linear array transducer (L7–4, Philips Healthcare, Andover, MA). A 200 or 400 μs toneburst at 4.09 MHz was focused at 19.7 mm with 64 active elements. This acoustic radiation force (ARF) push beam was centered in the aperture and centered laterally in the clot. After the ARF application, plane wave compounding was used for measuring the wave propagation. Three angled plane waves (−4°, 0°, +4°) with 5 MHz pulses were transmitted with a frame rate of 11.765 kHz were compounded, providing an effective frame rate of 3922 Hz (Montaldo *et al.*, 2009). The IQ data was saved for the compounded frames and motion estimation was performed using two-dimensional autocorrelation (Kasai *et al.*, 1985). The particle velocity was averaged over 1.5 mm of depth at surface of the clot and time-to-peak algorithm was used across multiple lateral positions to measure the shear wave group velocity (Palmeri *et al.*, 2008). Measurements were repeated five times for each clot without moving the transducer. Due to the ARF push beam being centered laterally in the clot, we measured the group velocity of left- and right-traveling waves. In the final analysis, assuming homogeneity of the clot, we pooled both results from the left and right waves and reported the mean value.

2.5 Dispersion Analysis

Due to the cylindrical shape of the clots and the differing diameters of the clots, we explored the possibility of guided waves being produced in the clots. We used the data from the OCE experiments for this analysis due to the measurements being confined to the surface, which made them more consistent for comparison. To effectively explore this guided wave aspect, we examined the phase velocity dispersion, or variation with frequency. We used the spatiotemporal data (t-x) used for the group velocity analysis and performed a two-dimensional Fourier transform to obtain a frequency domain representation with temporal and spatial frequency axes (f-k) (Bernal *et al.*, 2011). The coordinates of the peaks (f, k) in

the frequency domain distribution were identified to calculate the phase velocity using $c(f) = 2\pi f/k = \omega/k$. Dispersion curves were solved for a model of a solid cylinder in a vacuum of radius r and shear modulus μ, and were used to fit the measured dispersion curves to find the shear wave speed of the material using the relationship $c_s = \sqrt{\mu/\rho}$, where ρ is the mass density assumed to be 1000 kg/m^3.

The dispersion curves are obtained by modifying the semi-analytical finite element model proposed by Astaneh et al. (Astaneh *et al.*, 2017) for arterial walls, specialized by Roy and Guddati for incompressible elasticity to solid cylinders (Roy and Guddati, 2020). The model considers fully three-dimensional deformation yet uses finite element discretization only in the radial direction. Owing to the regular geometry, harmonic expansion is used in the other (temporal, axial and azimuthal) directions. The governing differential equation reduces to a quadratic eigenvalue problem, in terms of the axial wave number k, temporal frequency ω, eigenvector ϕ and circumferential wavenumber n

$$\left(k^2\boldsymbol{K}_2 + \boldsymbol{K}_0^{(n)} - \omega^2\boldsymbol{M}\right)\phi = 0 \tag{1}$$

For the case of homogeneous incompressible cylinder, it can be shown that the matrices $\boldsymbol{K}_2$ and $\boldsymbol{K}_0$ are proportional to μr and μ/r, respectively, i.e. $\boldsymbol{K}_2 = \mu r\bar{\boldsymbol{K}}_2$, $\boldsymbol{K}_0^{(n)} = \mu\bar{\boldsymbol{K}}_0^{(n)}/r$. Similarly, the mass matrix can be shown to be proportional to ρr, i.e. $\boldsymbol{M} = \rho r\bar{\boldsymbol{M}}$, where ρ is the density. Defining normalized phase velocity $\bar{c}_p = c_p/c_S$, and normalized frequency $\bar{\omega} = \omega r/c_S$, the eigenvalue problem in (1) can be written as

$$\left(\frac{\bar{\omega}^2}{\bar{c}_p{}^2}\bar{\boldsymbol{K}}_2 + \bar{\boldsymbol{K}}_0^{(n)} - \bar{\omega}^2\bar{\boldsymbol{M}}\right)\phi = 0 \tag{2}$$

The above problem is independent of geometric and material properties, and the normalized dispersion curve $\bar{c}_p(\bar{\omega})$ can be plotted as a universal curve shown in Fig. 2 in terms of the normalized phase velocity as a function of normalized frequency. Note that we get a single dispersion curve as we take the lowest eigenvalue associated with the first circumferential harmonic. In building the matrices in (2), due care is exercised to avoid volumetric locking using selective reduced integration (Roy and Guddati, 2020).

Owing to the ability to obtain universal dispersion curve in terms of normalized quantities that depend on the only unknown parameter C_S and known radius r, inversion for C_S becomes relatively straightforward. We first define the misfit as

$$f_{misfit} = \|c_p^s(c_S, f) - c_p^m(f)\|_2^2 \tag{3}$$

where, the least-squares norm is computed over the range of frequencies (f) where measured data is reliable. In this context, f is taken as 40 Hz to 140 Hz. The simulated values $\left(c_p^s\right)$ are obtained by simply scaling the normalized dispersion curve, and c_p^m represents the measured phase velocity. The misfit is minimized with the help of the Interior-point method with the

finite-difference gradient and the BFGS (Broyden-Fletcher-Goldfarb-Shanno) Hessian model. The MATLAB (Mathworks, Natick, MA) function *fmincon* is utilized with a positivity constraint to invert for the shear velocity C_S.

2.6 Statistical Analysis

All results are presented as the mean ± standard deviation (SD) of the wave velocities calculated using the GraphPad Prism Version 5 (GraphPad Software Inc., San Diego, USA). The D'Agostino & Pearson omnibus test and Shapiro-Wilk test were used to test for whether the wave velocity data from the clots were described by a normal distribution. In the study, the data was not normally distributed; therefore, nonparametric statistical tests were used to examine the significant differences between any two pairs of RBC compositions. To consider multiple comparisons in samples, the Kruskal–Wallis one-way analysis of variance test was used for comparing independent samples. In addition, Dunn's adjustment was implemented for adjusting the *p*-values in more strict condition to account for the situation of testing multiple comparisons. The Spearman correlation test was used to examine the correlation between OCE and SWE results. The significant differences were considered while the *p*-value was < 0.05.

3. Results

Histological evaluation was performed on each clot after OCE and SWE testing was completed. Images of representative samples of the clots are shown in Fig. 3. For each nominal mixture of RBC:fibrin, we took the mean value of the RBC content for plotting purposes. The RBC compositions of each Group were as follows – Group 1: 21% (averaged 23.5%, 19.7% and 18.7%), Group 2: 39% (averaged 41.8%, 38.6% and 36%), Group 3: 68% (averaged 65.9%, 68.5% and 69%), Group 4: 84% (averaged 82%, 85.8% and 84.9%) and Group 5: 95% (averaged 94.5%, 93.1% and 98.1%) from the histological examination.

The clots had a length of approximately 30 mm. The mean diameter of the clots placed on a Petri dish was 1.94 mm in 21% RBC, 2.64 mm in 39% RBC, 2.84 mm in 68% RBC, 3.78 mm in 84% RBC, and 5.36 mm in 95% RBC composition. Once the clots were pulled from the syringe, the clot keeps a cylindrical shape, but the volume of clots for each phenotype varied due to a variation in clot diameters resulting from increased contraction with increasing fibrin/platelet content (Johnson *et al.*, 2020). During the coagulation process, water was absorbed by the formed fibrin network and was stored within the swollen fibrin. However, these dimensions are in a similar range to those extracted during mechanical thrombectomy.

The wave velocities in the paper were reported with respect to the measured RBC compositions. Figures 4(a)–(b) illustrate the 39% RBC and 95% RBC B-mode images recorded by OCT. The backscatter signals display the substantial difference between 39% and 95% RBC composition. A larger backscatter signal can be observed under the surface of the 95% RBC clot, presented in Fig. 4(b). Due to the limited light penetration of the OCT in the clots, we were measuring Rayleigh waves on the clots because the wave propagation is traveling within approximately 0.5 mm under the clot surface. The shear wave speed can be calculated by multiplying by the approximate factor of 1.05 (Liu *et al.*, 2020a; Kirby *et al.*,

2017). Two-dimensional spatiotemporal wave motion maps are shown in Fig. 4(c) for 39% RBC and (d) for 95% RBC composition as examples. A group wave velocity was measured using the relationship between wave traveling distance and time as depicted by the black dashed line in Figs. 4(c)–(d). The mean wave group velocities of each RBC composition are exhibited in Fig. 4(e). We tested three individual clots in each RBC composition. The results demonstrated that the wave group velocity is significantly associated with the RBC compositions. The range of mean wave group velocity is as follows - Group 1 (21% RBC): from 0.66 ± 0.09 m/s to 0.91 ± 0.12 m/s, Group 2 (39% RBC): from 0.42 ± 0.05 m/s to 0.61 ± 0.03 m/s, Group 3 (68% RBC): from 0.43 ± 0.03 m/s to 0.64 ± 0.03 m/s, Group 4 (84% RBC): from 0.31 ± 0.01 m/s to 0.39 ± 0.01 m/s, and Group 5 (95% RBC): from 0.26 ± 0.01 to 0.33 ± 0.02 m/s. Based on the results, we demonstrated that the RBC compositions are inversely associated with the wave velocity measured in the clots. Furthermore, the combination of three individual samples for each RBC composition is illustrated in Fig. 5. The mean group velocity with its SD is 0.77 ± 0.15 for 21%, 0.49 ± 0.10 for 39%, 0.56 ± 0.10 for 68%, 0.34 ± 0.04 for 84% and 0.29 ± 0.03 for 95% RBC composition. The trend of wave group velocity is decreasing as RBC composition increased. Most clots were able to be distinguished by wave group velocity and showed a statistically significant difference between the clots with any two RBC compositions, except 39–68% and 84–95%.

In the SWE measurements, the wave measurement was not completely isolated to the surface as the OCE measurements were done. Example B-mode ultrasound images of the clots with 39% RBC and 95% RBC are shown in Figs. 6(a)–(b), respectively. The wave motion extracted from clots in Figs. 6(a)–(b) are shown in Figs. 6(c)–(d), respectively. The group velocity measured in the clots is summarized in Fig. 6(e) for each individual sample. Either 5–10 measurements are summarized for each sample. The mean group velocities measured by ultrasound of each RBC composition were exhibited in Fig. 6(e). Three samples for each RBC composition were tested. The results demonstrated that the shear wave group velocity is significantly associated with the RBC compositions except for the clots with 21% and 39% RBCs. The range of shear wave group velocity is from 0.19 ± 0.02 m/s to 0.43 ± 0.05 m/s for 21%, from 0.27 ± 0.01 m/s to 0.45 ± 0.18 m/s for 39%, from 0.39 ± 0.02 m/s to 0.52 ± 0.04 m/s for 68%, from 0.32 ± 0.01 m/s to 0.41 ± 0.03 m/s for 84%, and from 0.11 ± 0.01 to 0.30 ± 0.01 m/s for 95% RBC composition. The results demonstrated that the RBC compositions are inversely associated with the wave velocity of clots. Fig. 7 shows the results after samples from each mixture were grouped together. The mean group velocity with its SD is 0.32 ± 0.11 for 21%, 0.34 ± 0.14 for 39%, 0.44 ± 0.07 for 68%, 0.38 ± 0.04 for 84% and 0.21 ± 0.08 for 95% RBC composition. The trend of wave group velocity is decreasing with RBC composition increased from 68% to 95%. The clots can be distinguished by shear wave group velocity and showed a statistically significant difference between the clots with any two RBC compositions except 21–39%, 21–84%, 39–84% and 68–84%. We observed that OCE could be superior to SWE for characterizing clot compositions due to better spatial resolution.

We evaluated the correlation between OCE and SWE results that are shown in Fig. 8. The Spearman's correlation coefficient r is 0.432 for considering five RBC compositions illustrated in Fig. 8(a); however, it improved to 0.706 for the compositions from 39% to 95% as presented in Fig. 8(b). The low correlation coefficient ($r = 0.432$) was caused by the low

SWE measurement of group velocities for the 21% RBC composition. The small diameter of the 21% RBC clots may contribute to the disagreement between the OCE and SWE results. When clots with larger diameters were used, the correlation was higher ($r = 0.706$, $p = 0.013$). Another finding was that the results measured by using both modalities show the wave velocity for the 68% composition was faster than for the 39% composition.

Figure 9(a) shows the mean dispersion curve versus frequency for each RBC composition from the three samples and 10 acquisitions for the OCE data fit to the lowest order dispersion curve for the normalized characteristic dispersion curves. The shear wave phase velocities with SDs for the 21, 39, 68, 84, and 95% RBC compositions were 1.52 ± 0.48 m/s, 0.62 ± 0.10 m/s, 0.82 ± 0.24 m/s, 0.43 ± 0.05 m/s, and 0.34 ± 0.03 m/s, respectively, presented in Fig. 9(c). In an alternative depiction in Fig. 9(b), the overlaid data on the normalized characteristic curve demonstrates how the data lies on different sections of the curve due to incorporating the effects of frequency, radius, and shear wave velocity on the horizontal axis. However, we still observe that the clots with a 68% RBC composition have a higher shear wave velocity compared to those with the 39% RBC composition.

4. Discussion

In this study we demonstrated that elastographic evaluation may provide differentiation of clots created with different compositions of RBC. The OCE group velocity could distinguish between clots of different RBC compositions (Fig. 5). The ultrasound SWE group velocity did not have the same level of differentiation as the OCE results (Fig. 7), and this may have been linked to the incorporation of more depth information in the SWE results as the SWE method could visualize the waves throughout the thickness of the clot and used depth-based averaging for estimating the group velocity. In contrast, the OCE measurements were only performed at the surface of the clot. As a result, the SWE results may be more susceptible to including more complicated wave behavior particularly with the changing diameters of the clots from different RBC compositions.

We did find that the group velocities from the OCE and SWE methods were well correlated when we considered RBC compositions ≥ 39% (Fig. 8). RBC-rich clots, previously defined as > 50% RBC, will increase the stability in wave motion measurement because RBCs are strong scatterers for both OCT and ultrasound. This is despite a finding that the clot wave velocities were found to be higher in the 68% RBC composition group compared to the 39% RBC composition group. The 39% group could be an outlier in this study due to small amount of the samples and challenging to consistently separate with identical RBC counts from centrifuging human whole blood. The human whole blood has variance in composition from batch to batch. Besides, the rate of water extracting from the fibrin network could be different. More samples in each RBC composition will need to be tested in future work.

To try to decouple the effects of guided waves due to varying geometry of the clots and the measured wave speeds, we conducted dispersion analysis assuming a cylindrical geometry with a uniform shear modulus. The inversion provided good separation of the different clot types both in the conventional dispersion curves (phase velocities versus frequencies) and when superimposed on the normalized dispersion curve. The advantage of the dispersion

analysis is that we retrieve the shear wave velocity for the clot without having complications of geometry.

The elastographic evaluation of clots provided results that we could differentiate clots with different RBC compositions on a quantitative basis. The RBC-rich clots were softer by touch and had lower wave velocities. The fibrin-rich clots were considered to be stiffer by touch and generally had higher wave velocities. It was possible to differentiate the clots better with the OCE data compared to the SWE data, likely due to the spatial averaging that was performed with the ultrasound transducer being used. Using a higher frequency ultrasound transducer may have allowed for better spatial resolution and better differentiation, but it is more difficult to use ARF with higher frequency array transducers due to the potential harm it could pose to the transducer through element heating.

There are a few limitations of this study. We did note that the variability of both OCE and SWE measurements increased as the RBC content decreased. As the RBC content decreases, the amount of scattering for optical or ultrasound measurements decreases and the wave motion has more variability due to lower signal-to-noise ratio for motion estimation. We did note that within individual clots that the precision was reasonably high for most samples for RBC content >21% for OCE and for most clots measured with SWE except for one clot. In this study, we tested only three samples for each RBC composition where we did observe some variability within a given composition group, most notably 21%, 39% and 68%. In subsequent work, we need to test more sample clots for a given composition. It is also known that platelet content of a clot may be the most revealing factor in determining a clot's etiology, imaging features and revascularization outcome. Platelet-rich clots are associated with a large artery atherosclerosis source and are less likely to be completely revascularized with aspiration alone (Brinjikji *et al.*, 2020). Discovering platelets-rich clots analogues will be performed in future studies.

In this study, both the dimensions and mechanical properties were changing as a function of RBC content, which could complicate the interpretation of the group velocity results. The group velocity is a weighted average of phase velocities over a range of frequencies, so depending on how significantly the phase velocity is changing, the group velocity could be affected in a fairly sensitive manner. That is why we used the phase velocity dispersion analysis to attempt to decouple the geometry and mechanical properties and obtain a more accurate value of shear wave velocity.

We unfortunately did not perform mechanical testing with these clots so we do not have an independent measurement of the mechanical properties. Phantom tests would be difficult to perform for the entire range of mechanical properties evaluated as most tissue-mimicking materials will not support a self-supporting cylindrical form, particularly to mimic the high RBC content clots. As a result, we did not perform phantom tests that could match the size and mechanical property ranges for these clots. In future studies, we will explore different materials that could be used and potentially perform phantom measurements with similar sizes and mechanical properties for the clots that were tested. Again, our dispersion analysis was performed to attempt to decouple the geometry and mechanical properties using the OCE surface wave measurements.

The elastographic evaluations were performed in laboratory settings that are not amenable to clinical translation in the stroke patient due to limitations of performing these measurements deep in the tissue and through the skull. For effective translation of elastography to be applied for clot characterization in the stroke patient, a catheter-based implementation will need to be used. This could involve the combination of ultrasound and OCT technologies to generate a wave or perturbation and use ultrasound or OCT to measure the motion. The catheter would need a forward-facing orientation to interrogate the clot within the cross-section as opposed to the long side of the clot as was done in this study. Using higher frequency ultrasound would benefit the sensitivity of motion measurement within clots.

The dispersion analysis assumed a cylindrical geometry. The images in Figs. 4(a) and 6(a) show that as the RBC composition increases the surface becomes more regular and a cylindrical geometry assumption was more appropriate. Surface irregularity could have created some variability in the wave propagation and inversion results. A real clot embedded in a cylindrical vessel may conform better to the assumption of a regular cylinder.

5. Conclusions

We demonstrated that ARF-OCE and SWE are promising methods to explore the mechanical properties of human blood clots and to distinguish the clots with different RBC compositions by wave group velocities and dispersion analysis. For both ARF-OCE and SWE methods, the results showed trends of decreasing group velocities with higher RBC composition. Besides, the group velocities from the OCE and SWE methods were well correlated when RBC compositions were larger than 39%. In addition, the semi-analytical finite element model was used to explore the relationship between the phase velocities with various frequency ranges and radius of the clots. The inversion results showed that the trend of the shear wave velocity decreased with higher RBC composition. The ARF-OCE and SWE methods are able to provide elastographic characterization of blood clots. In future studies, platelet rich cases, clot-embedded vessels and catheter-based OCE or SWE will be considered for approaching more realistic situations for clinical translation.

Acknowledgements

This work was supported in part by the National Institutes of Health (R01 NS105853). The content is solely the responsibility of authors and does not necessarily represent the official views of the National Institute of Neurological Disorders and Stroke or the National Institutes of Health. The authors thank Mrs. Jennifer L. Poston for administrative assistance and Dr. Eric C. Polley for statistical analysis assistance.

References

Ambrozinski L, Song SZ, Yoon SJ, Pelivanov I, Li D, Gao L, Shen TT, Wang RKK and O'Donnell M 2016 Acoustic micro-tapping for non-contact 4D imaging of tissue elasticity Sci Rep-Uk 6

Astaneh AV, Urban MW, Aquino W, Greenleaf JF and Guddati MN 2017 Arterial waveguide model for shear wave elastography: implementation and in vitro validation Phys Med Biol 62 5473–94 [PubMed: 28609299]

Benson JC, Fitzgerald ST, Kadirvel R, Johnson C, Dai D, Karen D, Kallmes DF and Brinjikji W 2020 Clot permeability and histopathology: is a clot's perviousness on CT imaging correlated with its histologic composition? J Neurointerv Surg 12 38–42 [PubMed: 31239329]

Bernal M, Gennisson J-L, Flaud P and Tanter M 2012 Shear wave elastography quantification of blood elasticity during clotting Ultrasound Med. Biol 38 2218–28 [PubMed: 23069137]

Bernal M, Gennisson J-L, Flaud P and Tanter M 2013 Correlation between classical rheometry and supersonic shear wave imaging in blood clots Ultrasound Med. Biol 39 2123–36 [PubMed: 23972484]

Bernal M, Nenadic I, Urban MW and Greenleaf JF 2011 Material property estimation for tubes and arteries using ultrasound radiation force and analysis of propagating modes J Acoust Soc Am 129 1344–54 [PubMed: 21428498]

Bhatt M, Montagnon E, Destrempes F, Chayer B, Kazemirad S and Cloutier G 2018 Acoustic radiation force induced resonance elastography of coagulating blood: theoretical viscoelasticity modeling and ex-vivo experimentation Phys Med Biol

Brinjikji W, Fitzgerald S, Kallmes DF, Layton K, Hanel R, Pereira VM, Kvamme P, Delgado J, Yoo A, Jahromi B, Almekhlafi M, Gounis M and Nogueira RG 2020 Abstract 147: Outcomes of the Stroke Thromboembolism Registry of Imaging and Pathology: A Multicenter International Study Stroke 51 A147–A

Das S, Chandra Ghosh K, Malhotra M, Yadav U, Sankar Kundu S and Kumar Gangopadhyay P 2012 Short term mortality predictors in acute stroke Ann Neurosci 19 61–7 [PubMed: 25205967]

Doherty JR, Trahey GE, Nightingale KR and Palmeri ML 2013 Acoustic radiation force elasticity imaging in diagnostic ultrasound IEEE Trans. Ultrason. Ferroelectr. Freq. Control 60 685–701 [PubMed: 23549529]

Donnan GA, Fisher M, Macleod M and Davis SM 2008 Stroke Lancet 371 1612–23 [PubMed: 18468545]

Fennell VS, Setlur Nagesh SV, Meess KM, Gutierrez L, James RH, Springer ME and Siddiqui AH 2018 What to do about fibrin rich 'tough clots'? Comparing the Solitaire stent retriever with a novel geometric clot extractor in an in vitro stroke model J Neurointerv Surg 10 907–10 [PubMed: 29352061]

Fitzgerald S, Wang S, Dai D, Murphree DH Jr., Pandit A, Douglas A, Rizvi A, Kadirvel R, Gilvarry M, McCarthy R, Stritt M, Gounis MJ, Brinjikji W, Kallmes DF and Doyle KM 2019 Orbit image analysis machine learning software can be used for the histological quantification of acute ischemic stroke blood clots PLoS One 14 e0225841 [PubMed: 31805096]

Goyal M, Menon BK, van Zwam WH, Dippel DW, Mitchell PJ, Demchuk AM, Davalos A, Majoie CB, van der Lugt A, de Miquel MA, Donnan GA, Roos YB, Bonafe A, Jahan R, Diener HC, van den Berg LA, Levy EI, Berkhemer OA, Pereira VM, Rempel J, Millan M, Davis SM, Roy D, Thornton J, Roman LS, Ribo M, Beumer D, Stouch B, Brown S, Campbell BC, van Oostenbrugge RJ, Saver JL, Hill MD, Jovin TG and collaborators H 2016 Endovascular thrombectomy after large-vessel ischaemic stroke: a meta-analysis of individual patient data from five randomised trials Lancet 387 1723–31 [PubMed: 26898852]

Grau AJ, Weimar C, Buggle F, Heinrich A, Goertler M, Neumaier S, Glahn J, Brandt T, Hacke W and Diener HC 2001 Risk factors, outcome, and treatment in subtypes of ischemic stroke: the German stroke data bank Stroke 32 2559–66 [PubMed: 11692017]

Han ZL, Aglyamov SR, Li JS, Singh M, Wang S, Vantipalli S, Wu C, Liu CH, Twa MD and Larin KV 2015 Quantitative assessment of corneal viscoelasticity using optical coherence elastography and a modified Rayleigh-Lamb equation J Biomed Opt 20

Han ZL, Li JS, Singh M, Wu C, Liu CH, Raghunathan R, Aglyamov SR, Vantipalli S, Twa MD and Larin KV 2017 Optical coherence elastography assessment of corneal viscoelasticity with a modified Rayleigh-Lamb wave model J Mech Behav Biomed 66 87–94

Hashimoto T, Hayakawa M, Funatsu N, Yamagami H, Satow T, Takahashi JC, Nagatsuka K, Ishibashi-Ueda H, Kira JI and Toyoda K 2016 Histopathologic Analysis of Retrieved Thrombi Associated With Successful Reperfusion After Acute Stroke Thrombectomy Stroke 47 3035–7 [PubMed: 27780903]

Hoang P, Wallace A, Sugi M, Fleck A, Pershad Y, Dahiya N, Albadawi H, Knuttinen G, Naidu S and Oklu R 2017 Elastography techniques in the evaluation of deep vein thrombosis Cardiovasc Diagn Ther 7 S238–S45 [PubMed: 29399527]

Johnson S, Chueh J, Gounis MJ, McCarthy R, McGarry JP, McHugh PE and Gilvarry M 2020 Mechanical behavior of in vitro blood clots and the implications for acute ischemic stroke treatment J Neurointerv Surg 12 853–7 [PubMed: 31780453]

Jorgensen AS, Rasmussen AM, Andersen NKM, Andersen SK, Emborg J, Roge R and Ostergaard LR 2017 Using cell nuclei features to detect colon cancer tissue in hematoxylin and eosin stained slides Cytom Part A 91a 785–93

Kasai C, Namekawa K, Koyano A and Omoto R 1985 Real-time two-dimensional blood flow imaging using an autocorrelation technique IEEE Trans. Son. Ultrason SU-32 458–64

Kirby MA, Pelivanov I, Song S, Ambrozinski L, Yoon SJ, Gao L, Li D, Shen TT, Wang RK and O'Donnell M 2017 Optical coherence elastography in ophthalmology J Biomed Opt 22 1–28

Li CH, Guan GY, Li SA, Huang ZH and Wang RK 2012a Evaluating elastic properties of heterogeneous soft tissue by surface acoustic waves detected by phase-sensitive optical coherence tomography J Biomed Opt 17

Li CH, Guan GY, Ling YT, Hsu YT, Song SZ, Huang JTJ, Lang S, Wang RKK, Huang ZH and Nabi G 2015 Detection and characterisation of biopsy tissue using quantitative optical coherence elastography (OCE) in men with suspected prostate cancer Cancer Lett 357 121–8 [PubMed: 25444932]

Li CH, Guan GY, Reif R, Huang ZH and Wang RKK 2012b Determining elastic properties of skin by measuring surface waves from an impulse mechanical stimulus using phase-sensitive optical coherence tomography J R Soc Interface 9 831–41 [PubMed: 22048946]

Liang X, Adie SG, John R and Boppart SA 2010 Dynamic spectral-domain optical coherence elastography for tissue characterization Opt Express 18 14183–90 [PubMed: 20588552]

Liu HC, Kijanka P and Urban MW 2020a Acoustic radiation force optical coherence elastography for evaluating mechanical properties of soft condensed matters and its biological applications Journal of biophotonics 13 e201960134 [PubMed: 31872545]

Liu HC, Kijanka P and Urban MW 2020b Optical coherence tomography for evaluating capillary waves in blood and plasma Biomed Opt Express 11 1092–106 [PubMed: 32206401]

Liu X, Li N and Wen C 2017 Effect of pathological heterogeneity on shear wave elasticity imaging in the staging of deep venous thrombosis PLOS ONE 12 e0179103 [PubMed: 28614362]

Manapuram RK, Baranov SA, Manne VGR, Sudheendran N, Mashiatulla M, Aglyamov S, Emelianov S and Larin KV 2011 Assessment of wave propagation on surfaces of crystalline lens with phase sensitive optical coherence tomography Laser Phys Lett 8 164–8

Mercado-Shekhar KP, Kleven RT, Aponte Rivera H, Lewis R, Karani KB, Vos HJ, Abruzzo TA, Haworth KJ and Holland CK 2018 Effect of Clot Stiffness on Recombinant Tissue Plasminogen Activator Lytic Susceptibility in Vitro Ultrasound Med. Biol 44 2710–27 [PubMed: 30268531]

Mfoumou E, Tripette J, Blostein M and Cloutier G 2014 Time-dependent hardening of blood clots quantitatively measured in vivo with shear-wave ultrasound imaging in a rabbit model of venous thrombosis Thrombosis Research 133 265–71 [PubMed: 24315316]

Montaldo G, Tanter M, Bercoff J, Benech N and Fink M 2009 Coherent plane-wave compounding for very high frame rate ultrasonography and transient elastography IEEE Transactions on Ultrasonics Ferroelectrics and Frequency Control 56 489–506

Montaner J, Perea-Gainza M, Delgado P, Ribo M, Chacon P, Rosell A, Quintana M, Palacios ME, Molina CA and Alvarez-Sabin J 2008 Etiologic diagnosis of ischemic stroke subtypes with plasma biomarkers Stroke 39 2280–7 [PubMed: 18535284]

Palmeri ML, Wang MH, Dahl JJ, Frinkley KD and Nightingale KR 2008 Quantifying hepatic shear modulus in vivo using acoustic radiation force Ultrasound in Medicine and Biology 34 546–58 [PubMed: 18222031]

Powers WJ, Derdeyn CP, Biller J, Coffey CS, Hoh BL, Jauch EC, Johnston KC, Johnston SC, Khalessi AA, Kidwell CS, Meschia JF, Ovbiagele B, Yavagal DR and American Heart Association Stroke C 2015 2015 American Heart Association/American Stroke Association Focused Update of the 2013 Guidelines for the Early Management of Patients With Acute Ischemic Stroke Regarding Endovascular Treatment: A Guideline for Healthcare Professionals From the American Heart Association/American Stroke Association Stroke 46 3020–35 [PubMed: 26123479]

Raychev R and Saver JL 2012 Mechanical thrombectomy devices for treatment of stroke Neurol Clin Pract 2 231–5 [PubMed: 23634369]

Razani M, Mariampillai A, Sun CR, Luk TWH, Yang VXD and Kolios MC 2012 Feasibility of optical coherence elastography measurements of shear wave propagation in homogeneous tissue equivalent phantoms Biomedical Optics Express 3 972–80 [PubMed: 22567590]

Roy T and Guddati MN 2020 Shear Wave Dispersion Analysis of Incompressible Waveguides submitted to Journal of the Acoustical Society of America

Rubin JM, Aglyamov SR, Wakefield TW, O'Donnell M and Emelianov SY 2003 Clinical application of sonographic elasticity imaging for aging of deep venous thrombosis: preliminary findings J Ultrasound Med 22 443–8 [PubMed: 12751855]

Rubin JM, Xie H, Kim K, Weitzel WF, Emelianov SY, Aglyamov SR, Wakefield TW, Urquhart AG and O'Donnell M 2006 Sonographic elasticity imaging of acute and chronic deep venous thrombosis in humans J Ultrasound Med 25 1179–86 [PubMed: 16929019]

Sarvazyan A, Hall TJ, Urban MW, Fatemi M, Aglyamov SR and Garra B 2011 Elasticity imaging - an emerging branch of medical imaging. An overview. Curr. Med. Imaging Rev 7 255–82 [PubMed: 22308105]

Sarvazyan AP, Rudenko OV, Swanson SD, Fowlkes JB and Emelianov SY 1998 Shear wave elasticity imaging: a new ultrasonic technology of medical diagnostics Ultrasound Med. Biol 24 1419–35 [PubMed: 10385964]

Schmitt C, Hadj Henni A and Cloutier G 2011 Characterization of blood clot viscoelasticity by dynamic ultrasound elastography and modeling of the rheological behavior J Biomech 44 622–9 [PubMed: 21122863]

Undas A, Slowik A, Wolkow P, Szczudlik A and Tracz W 2010 Fibrin clot properties in acute ischemic stroke: relation to neurological deficit Thromb Res 125 357–61 [PubMed: 19942259]

Urban MW 2018 Production of acoustic radiation force using ultrasound: methods and applications Expert Review of Medical Devices 15 819–34 [PubMed: 30350736]

Viola F, Kramer MD, Lawrence MB, Oberhauser JP and Walker WF 2004 Sonorheometry: a noncontact method for the dynamic assessment of thrombosis Ann Biomed Eng 32 696–705 [PubMed: 15171624]

Wang CW, Perez MJ, Helmke BP, Viola F and Lawrence MB 2015 Integration of acoustic radiation force and optical imaging for blood plasma clot stiffness measurement PLoS One 10 e0128799 [PubMed: 26042775]

Wang S and Larin KV 2015 Optical coherence elastography for tissue characterization: a review J Biophotonics 8 279–302 [PubMed: 25412100]

Xie H, Kim K, Aglyamov SR, Emelianov SY, O'Donnell M, Weitzel WF, Wrobleski SK, Myers DD, Wakefield TW and Rubin JM 2005 Correspondence of ultrasound elasticity imaging to direct mechanical measurement in aging DVT in rats Ultrasound Med Biol 31 1351–9 [PubMed: 16223638]

Xu X, Zhu J and Chen Z 2016 Dynamic and quantitative assessment of blood coagulation using optical coherence elastography Sci Rep 6 24294 [PubMed: 27090437]

Xu X, Zhu J, Yu J and Chen Z 2019 Viscosity monitoring during hemodiluted blood coagulation using optical coherence elastography IEEE J Sel Top Quantum Electron 25

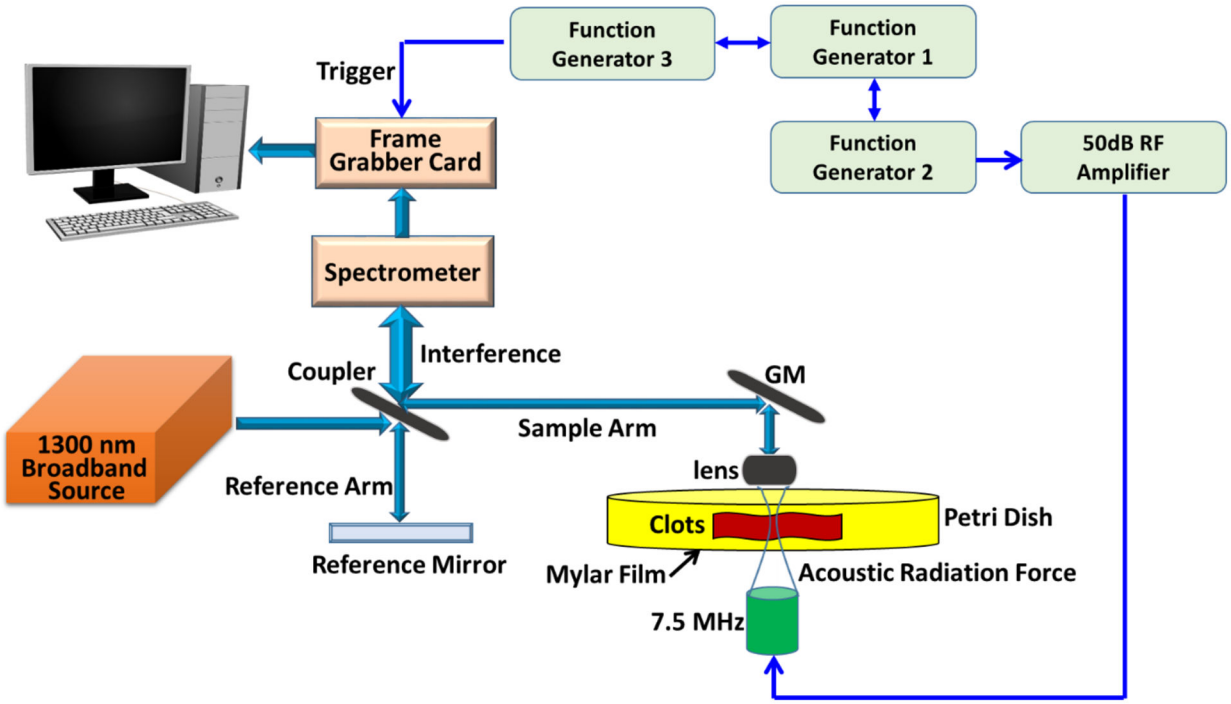

FIG. 1.

Schematic of acoustic radiation forced optical coherence tomography (ARF-OCT). GM and RF represent galvanometer mirror and radio frequency, respectively. The three function generators are utilized to provide trigger and driving signals for synchronizing OCT scan, excitation and recording signals.

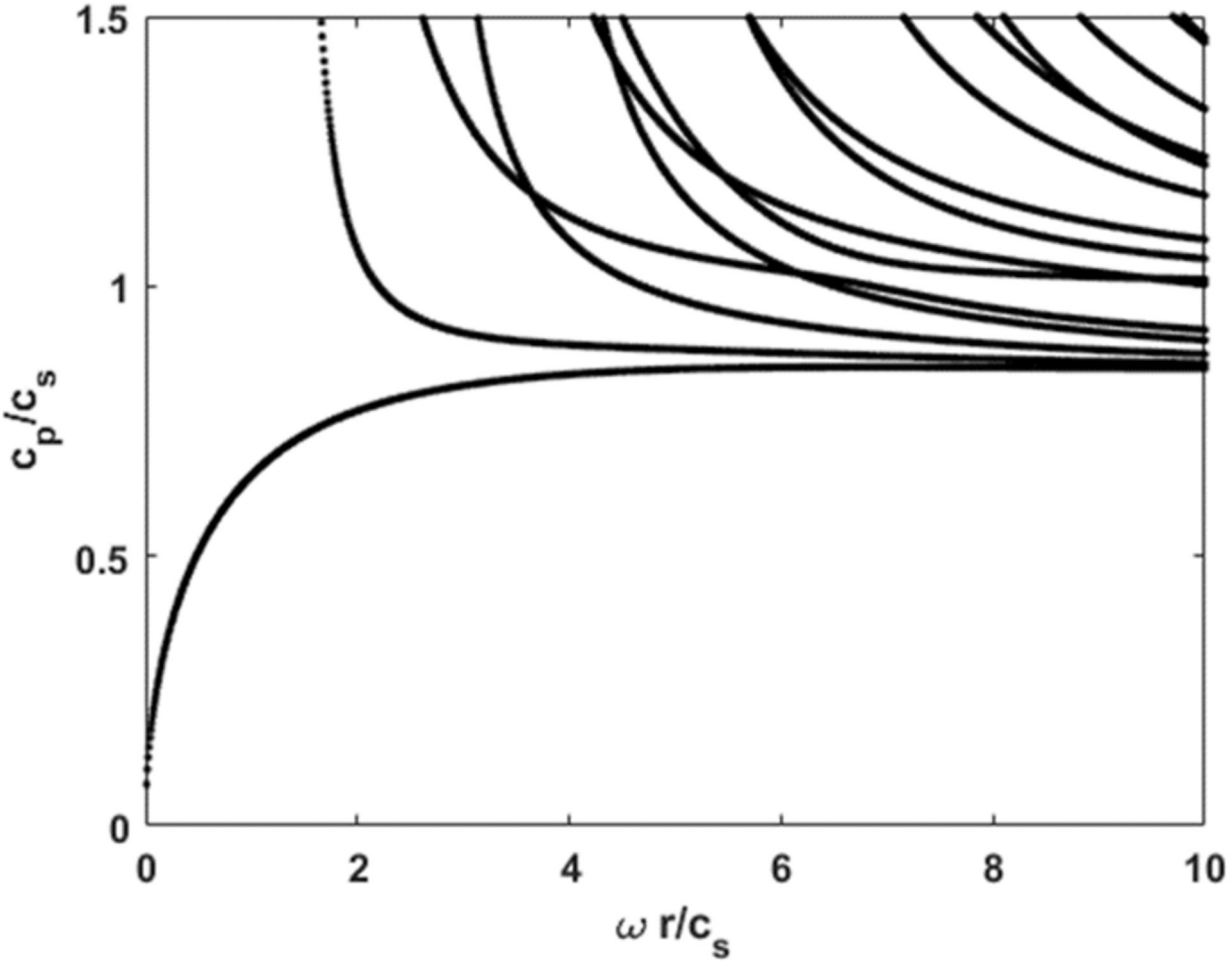

FIG. 2.

The normalized dispersion curves for solid cylinder with three-dimensional deformation situation by using semi-analytical finite element theoretical calculations.

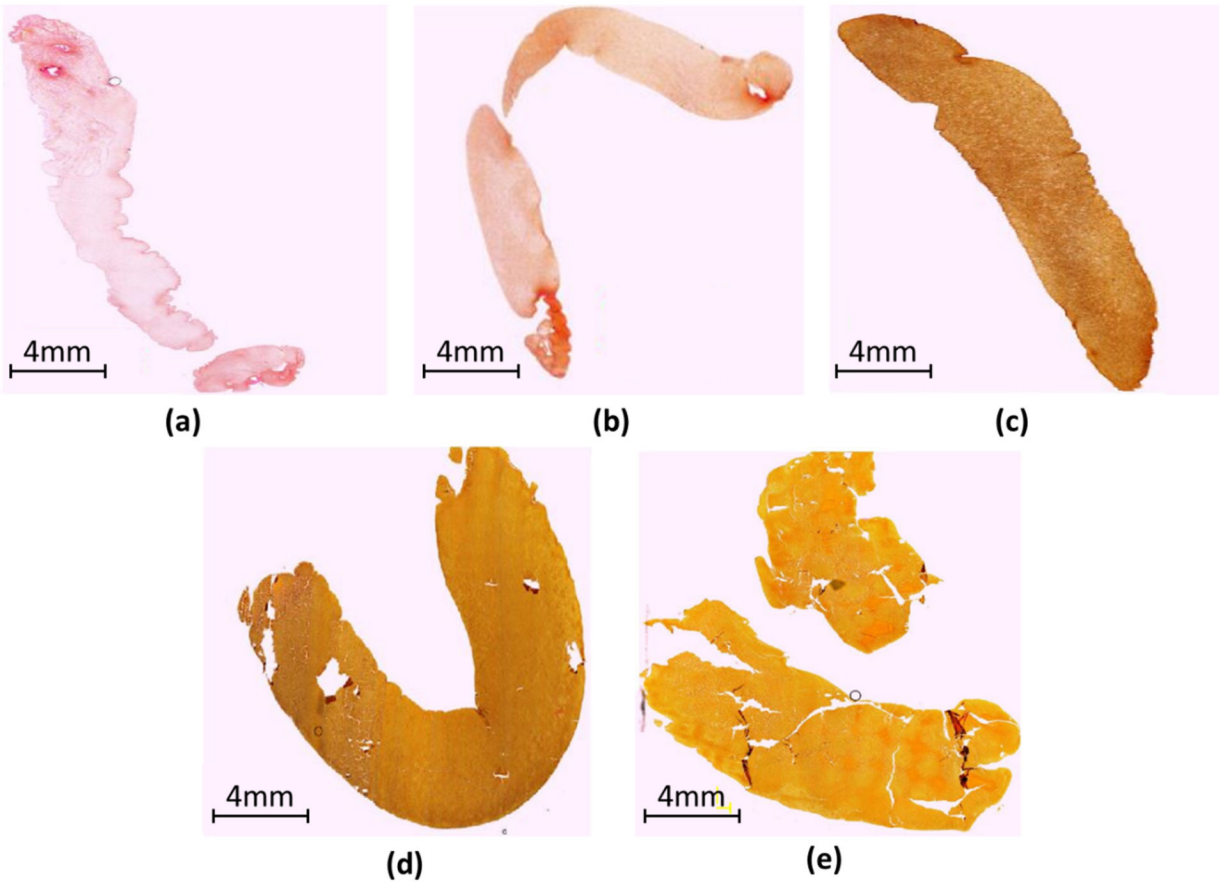

FIG. 3.

Histological examination of the clots with representative examples for the following RBC compositions. (a) 21% RBC, (b) 39% RBC, (c) 68% RBC, (d) 84% RBC and (e) 95% RBC.

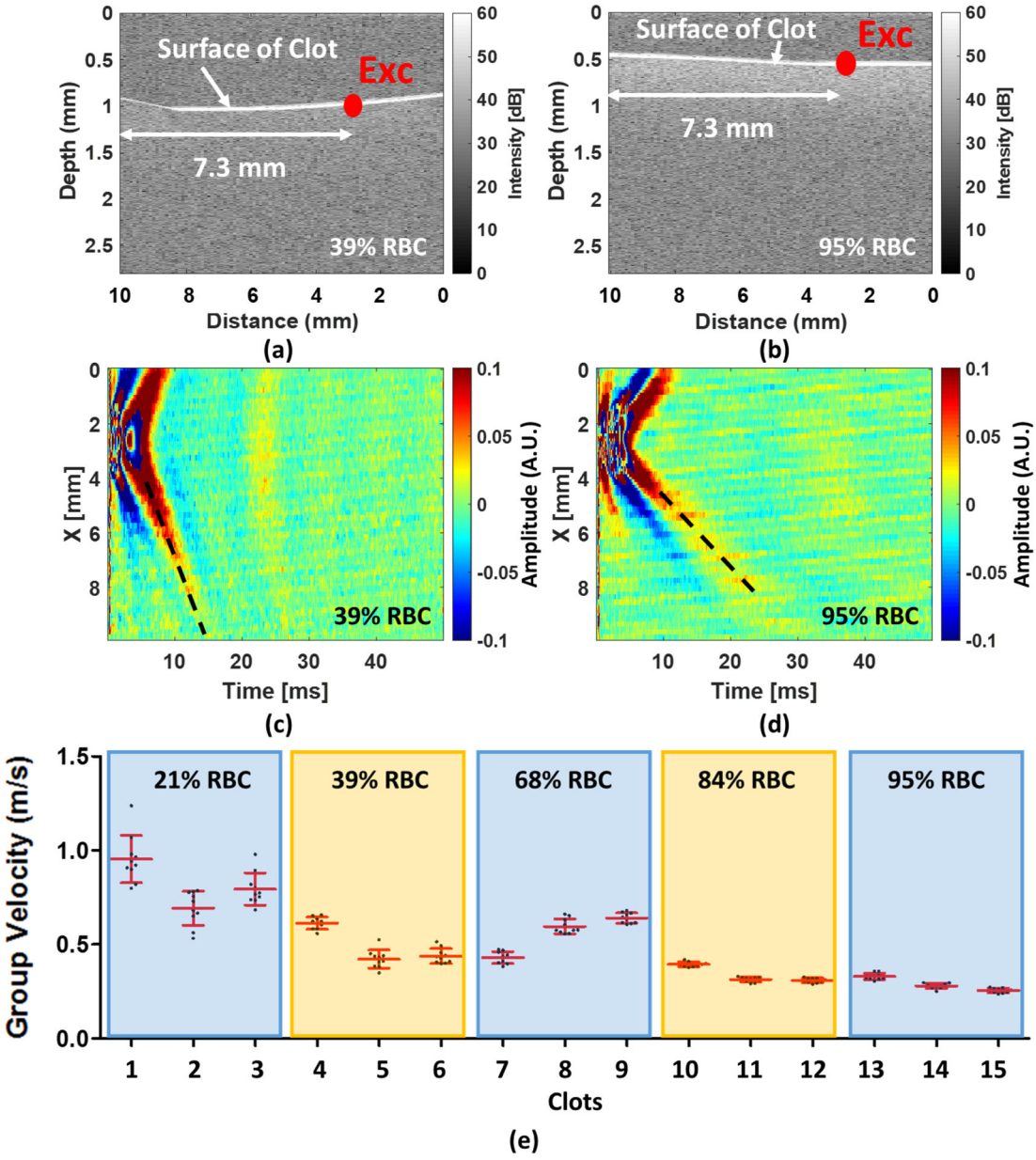

FIG. 4.

(a) and (b) An example shows the 39% and 95% RBC composition of an OCT image composed by using IQ data, respectively. (c) and (d) A 2D spatiotemporal wave map of wave motion in 39% and 95% RBC composition, respectively. (e) The mean group velocity with their SDs for each RBC composition. The Exc in (a) and (b) denotes the ultrasound excitation location.

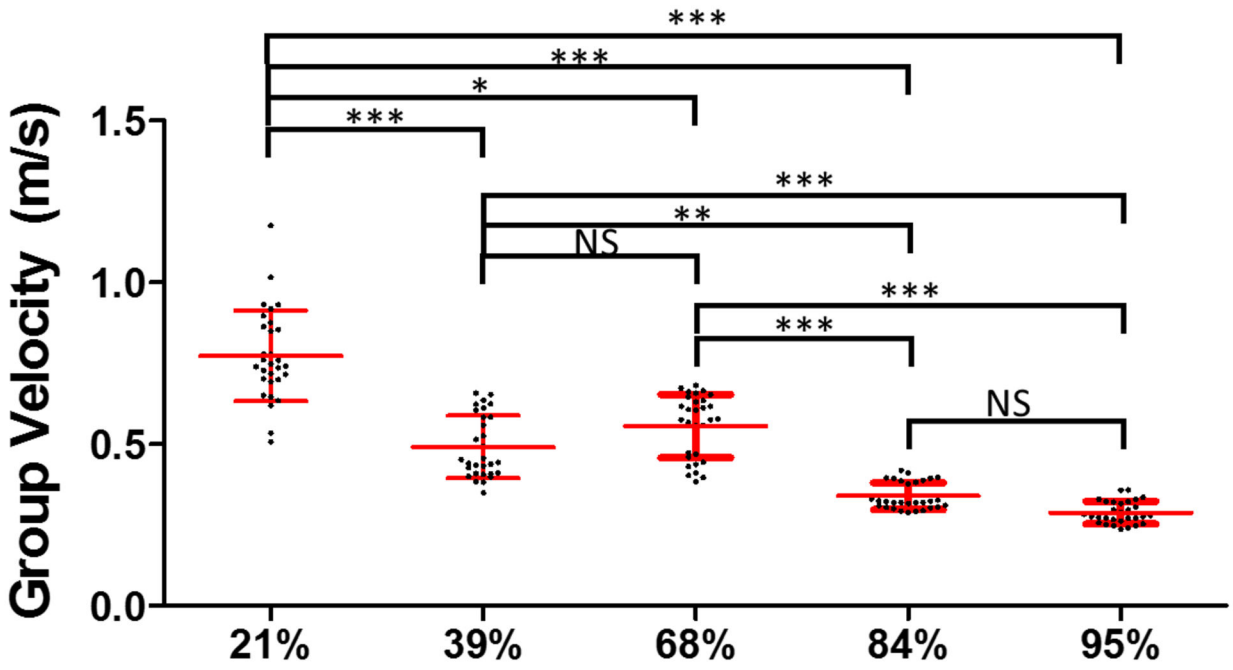

FIG. 5.

The combination of three individual samples for each RBC compositions, measured by ARF-OCE. The symbols ***, ** and * indicate the *p*-value < 0.001, < 0.01 and < 0.05, respectively. The notation NS means non-significant ($p > 0.05$).

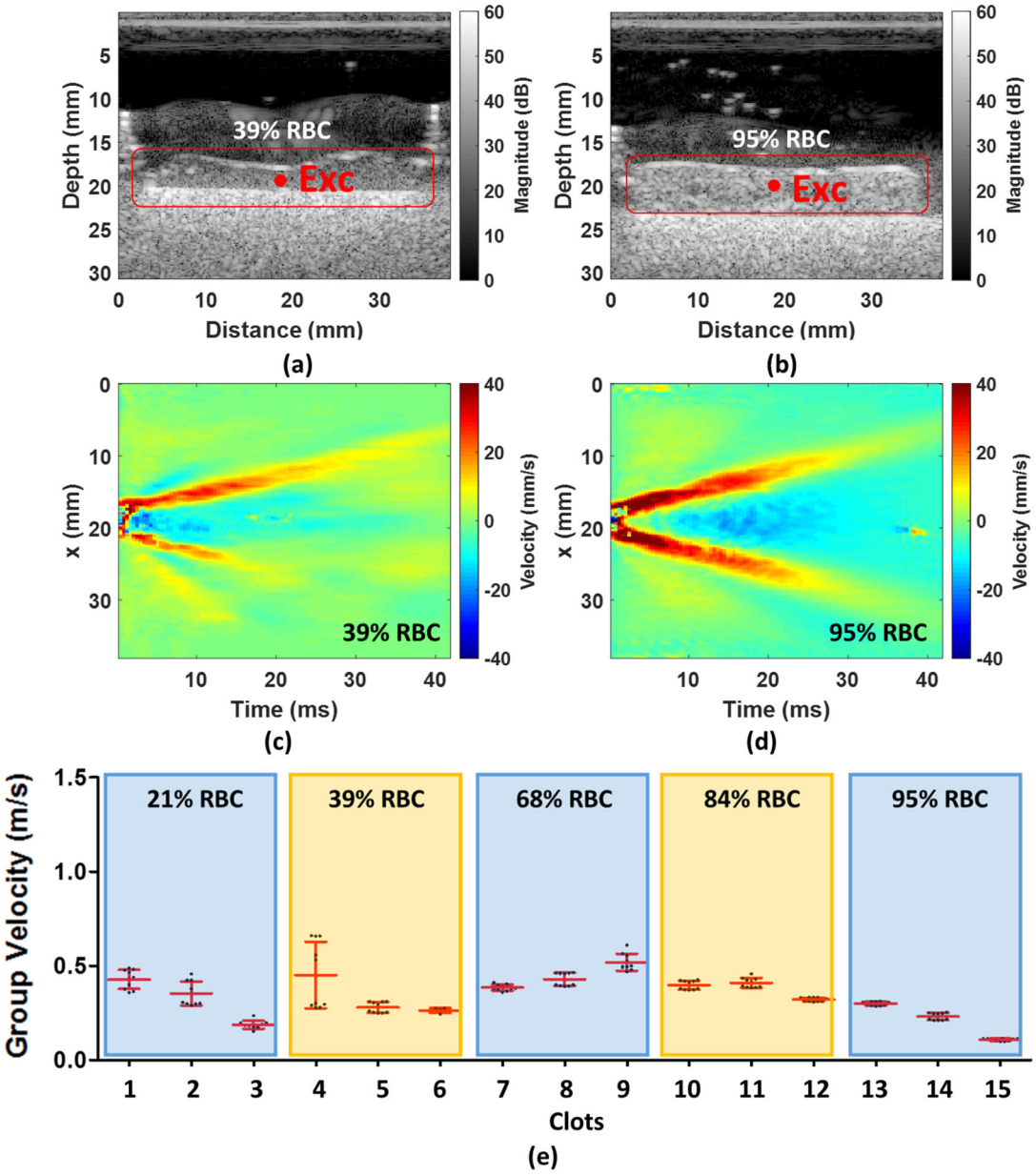

FIG. 6.

(a) and (b) An example shows the 39% and 95% RBC composition of ultrasound B-mode image, respectively. (c) and (d) A 2D a lateral time-peak wave map of wave motion in 39% and 95% RBC composition, respectively. (e) The mean group velocity with their SDs for each RBC composition. The Exc in (a) and (b) denotes the ultrasound excitation location.

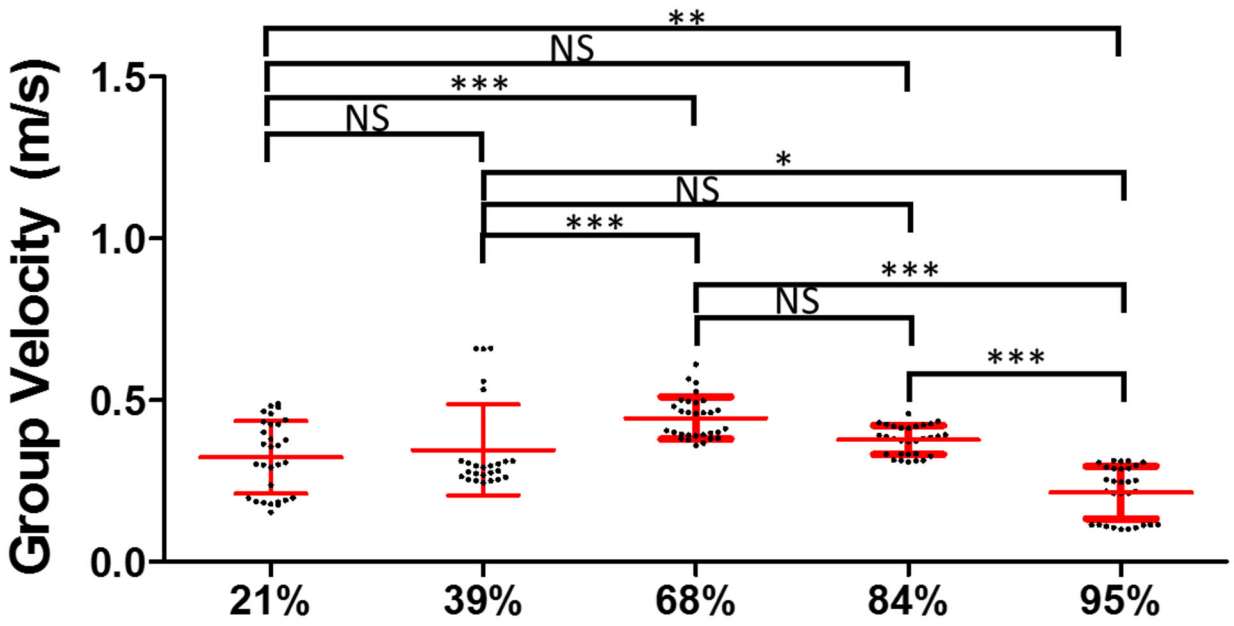

FIG. 7.

The combination of three individual samples for each RBC compositions, measured by SWE. ***, ** and * indicate the *p*-value < 0.001, < 0.01 and < 0.05, respectively. The notation NS means non-significant ($p > 0.05$).

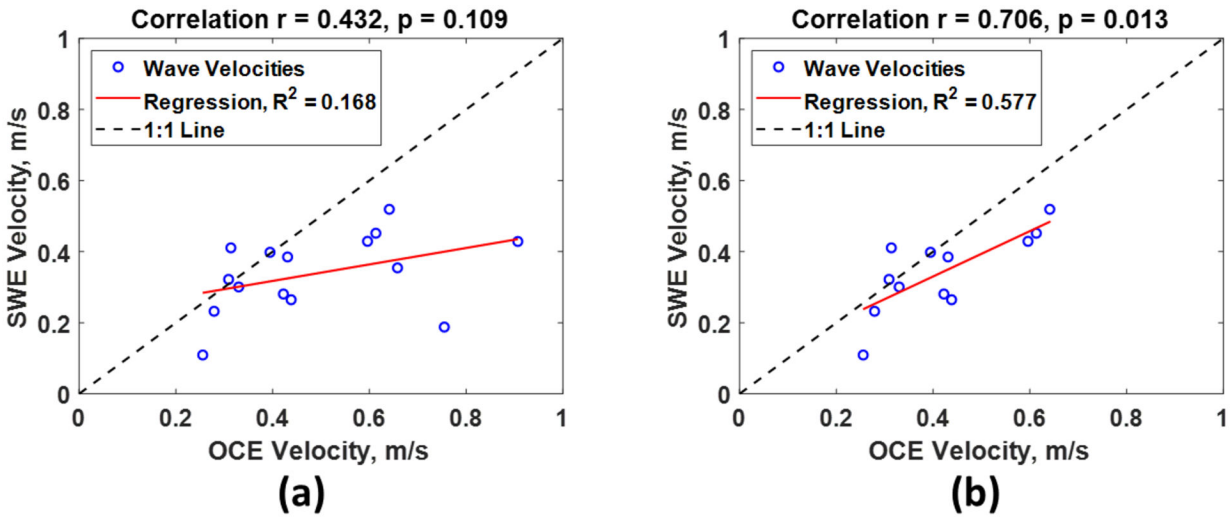

FIG. 8.

The Spearman correlation between OCE and SWE results that are shown in (a) for the compositions from 21% to 95%, (b) for the compositions from 39% to 95%.

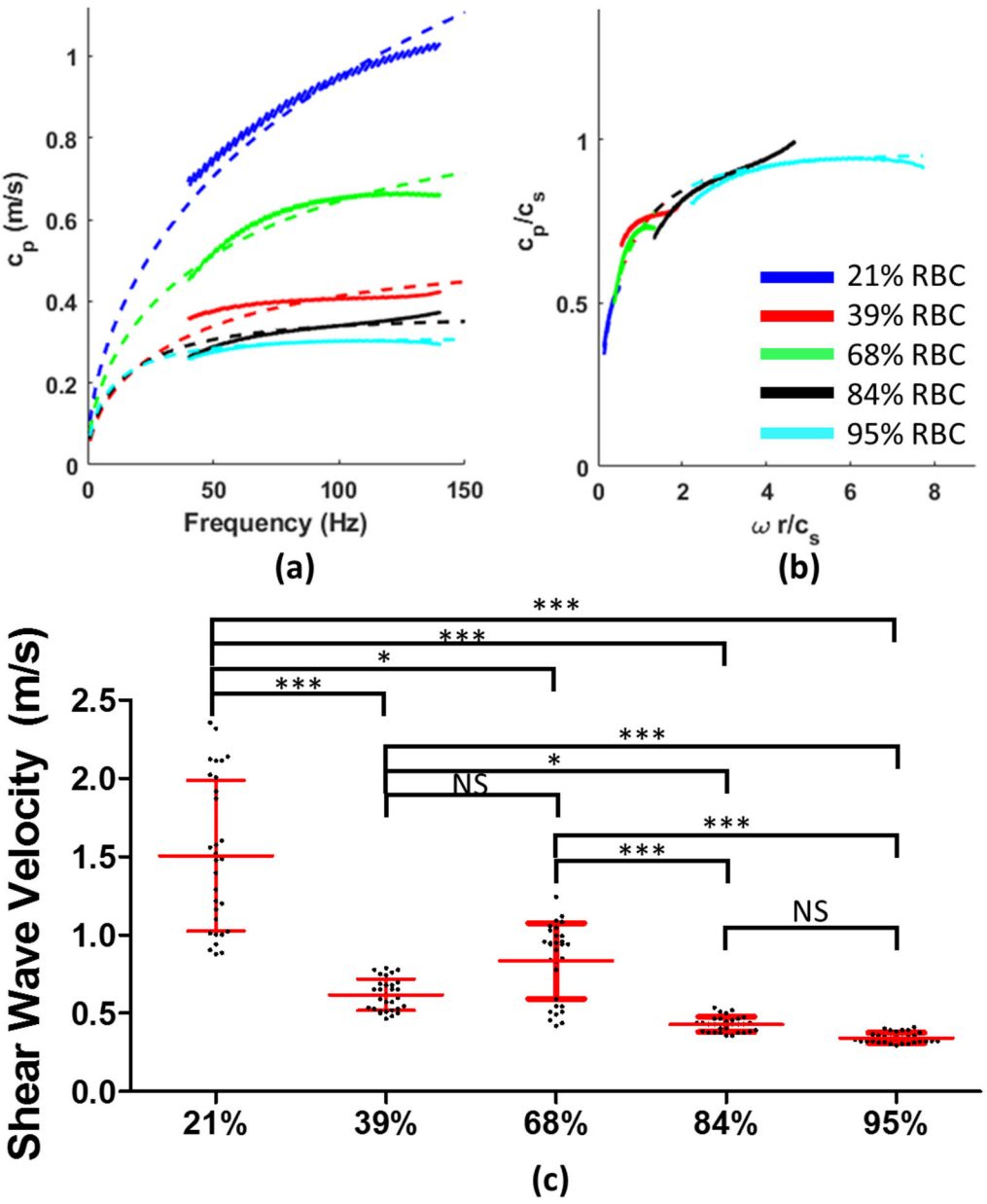

FIG. 9.

OCE dispersion analysis results. The match with the measured and computed dispersion curves with the inverted shear wave velocities. (a) shows the match in the physical space and (b) shows the match in the normalized space. The mean with SD for five RBC compositions were presented in (c). The symbol ***, ** and * indicate the *p*-value < 0.001, < 0.01 and < 0.05, respectively. The notation NS means non-significant ($p > 0.05$).